3D Semantic Segmentation-Driven Representations for 3D Object Detection

Hayeon O¹ and Kunsoo Huh²

Department of Automotive Engineering (Automotive-Computer Convergence)

Department of Automotive Engineering

Hanyang University, Seoul, 04763, Republic of Korea

{gkdus9595, khuh2}@hanyang.ac.kr

Abstract. In autonomous driving, 3D detection provides more precise information to downstream tasks, including path planning and motion estimation, compared to 2D detection. Therefore, the need for 3D detection research has emerged. However, although single and multi-view images and depth maps obtained from the camera were used, detection accuracy was relatively low compared to other modality-based detectors due to the lack of geometric information. The proposed multi-modal 3D object detection combines semantic features obtained from images and geometric features obtained from point clouds, but there are difficulties in defining unified representation to fuse data existing in different domains and synchronization between them. In this paper, we propose SeSame: point-wise semantic feature as a new presentation to ensure sufficient semantic information of the existing LiDAR-only based 3D detection. Experiments show that our approach outperforms previous state-of-the-art at different levels of difficulty in car and performance improvement on the KITTI object detection benchmark. Our code is available at https://github.com/HAMA-DL-dev/SeSame

Keywords: semantic segmentation \cdot 3D object detection \cdot autonomous driving

1 Introduction

The autonomous driving system is structured in a sequential flow where preceding tasks influence subsequent ones. As the perception system is the initial step in identifying the surrounding environment for autonomous driving, it bears the responsibility of providing accurate information to downstream tasks, e.g. decision-making, path planning, and control. Therefore, various tasks for recognizing driving situations using cameras and LiDAR have been proposed. Notably, 2D detection based on image from camera has achieved accuracy surpassing human identification capabilities due to the rapid advancement of deep learning and ongoing research. However, it has limitations in conveying height and shape information about objects, hindering the delivery of precise information. For this reason, the importance of 3D object detection has emerged. Moreover, according

to [20, 28], this provides advantages in representing 3D detection results in the Bird's-Eye View (BEV), where the BEV plane acts as the global coordinate for downstream tasks in autonomous driving. In other words, accurate results from 3D detection also enhance the precision of downstream tasks. For these reasons, 3D object detection is indispensable in autonomous driving.

Image-based 3D object detection aims to overcome the limitations of image, which lacks depth information, by estimating depth and generating pseudo-LiDAR point clouds [31]. Nevertheless, this approach tends to have lower accuracy compared to LiDAR-only 3D detection based on point clouds, and employing multi-view images to enhance precision increases significant computational cost. Consequently, other fusion methods have been proposed, which combine point clouds with images and are categorized into early [23,30], deep [8,11,13,18], and late fusion [21] based on when and how they are fused. But, the multimodality method presents challenges in integrating and synchronizing data, which have different representations and are defined in different coordinate systems. On the other hand, LiDAR-only-based 3D object detection has the advantage of fully leveraging the geometric information provided by point cloud. hile point clouds may lack semantic information compared to images, early research in 3D semantic segmentation has utilized range-view images from projecting point clouds, enabling the extraction of sufficient semantic features. This led to a question: "what if we can extract sufficient semantic features from point cloud and leverage them in existing 3D detectors?"

Therefore, inspired by the question and [30], this paper proposes a method to utilize semantic features obtained from 3D semantic segmentation as the representation for LiDAR-only 3D object detection, aiming to minimize loss and distortion on geometric information and preserve it. As illustrated in Fig. 3, this method consists of three components, where 3D semantic segmentation provides supplementary semantic features for 3D detector. The features are combined with raw point cloud through feature concatenation. Evaluation of proposed method based on the KITTI object detection dataset reveals the method outperforms multi-modal 3D object detection [8,13] for all classes and reference model [30] for car, in terms of metrics defined in the benchmark. In summary, the contributions of this paper are as follows: (1) We propose a novel representation for 3D object detectors by integrating segmented point cloud obtained from 3D semantic segmentation. To our best knowledge, it is the first to leverage semantic segmentation to object detection. (2) A detector in the proposed method, utilizing this representation, can be easily replaced. And this flexibility extends to various detectors that require different type of input feature for encoding. (3) The proposed method minimizing loss and distortion in the process of extracting and incorporating semantic features outperforms multi-modality approach for all classes, and the reference model and the baseline detector for car on KITTI object detection benchmark.

2 Related Works

2.1 Semantic Segmentation.

To fully understand the driving scenario in autonomous driving, precise semantic segmentation is required. Depending on the sensor; camera and LiDAR, semantic segmentation in autonomous driving can be divided into 2D semantic segmentation at the pixel-wise level and 3D semantic segmentation at the point-wise level [10]. The tasks perform multi-class classification on pixels and points that constitute image and point cloud, respectively.

2D semantic segmentation. Following the initial model of FCN [19], U-Net [26] is an architecture for semantic segmentation in medical image analvsis. [26] fully leverage features from each layer by dense skip connections, connecting features from each layer in the encoder part to symmetrical layers in the decoder part. The skip connection with a symmetric structure contributes to modeling relationship between pixels, allowing feature concatenation to perform semantic segmentation. It directly concatenates different levels of semantic features and is proven to be more efficient in image with irregular and coarse edges, like medical image. Iandola et al. [12] proposed a structure with squeeze and expand layers organized around replacing some 3x3 convolutional filters with 1x1 filters, suggesting fire-module to ensure accuracy while reducing parameters for efficiency. Subsequently, downsampling closer to the end of the network results in larger activation maps compared to previous methods, enhancing classification accuracy. Those approach focus on relationship between pixels rather than extracting features from them, influencing on 3D semantic segmentation for point cloud.

3D semantic segmentation. Originated from the PointNet series [24,25]; they are for indoor space, limiting their ability to extract semantic features from outdoor driving environments which have diverse density contexts. Thus, 3D semantic segmentation based on the 2D semantic segmentation is proposed to guarantee semantic features from point cloud. SqueezeSeg [33] and PointSeg [32], inspried by [12], utilize spherical projection to convert point cloud into rangeview image, apply 2D semantic segmentation, and then map the result back to the point cloud. However, spherical projection has the drawback of causing loss or distortion of semantic information from the camera and geometric information from the point cloud. Z.Zhuang et al. [38] address this limitation with twostream network(TSNet) and perspective projection. The TSNet takes as input image and point cloud projected with calibration matrix, returning a probabilistic semantic map and minimizing the perception-aware loss defined between them. Nevertheless, similar to Fig. 1, this method is sensitive to the calibration, and its slight variations can significantly affect the results [1]. Inspired by [26], Y.Zhang et al. [35] proposed BEV projection method to project point cloud onto a 2D grid. Unlike voxelization defined in Cartesian coordinate [36], this applies a polar coordinate system to encode point clouds. However, this method also

4 H.O, K.Huh

cannot fully preserve geometric information because it projects 3D point clouds into 2D space.

Cylinder3D [37], instead of other projection methods, converts point clouds defined in Cartesian coordinate into Cylindrical coordinate, considering the sparsity of point cloud. Two modules utilize the transformed features *i.e.* Asymmetrical Residual Block and Dimension-decomposition-based Context Modeling. The Asymmetrical Residual Block considers the characteristic of many objects in autonomous driving scenes being cuboid-shaped. The dimension-decomposition is proposed to consider the various contexts that point clouds represent in outdoor spaces with different densities. To reflect these high-rank contexts, they are divided according to context, enabling a 3D semantic segmentation that fully understands high-rank contexts while having low computational cost. In this paper, we propose a method to improve 3D object detection performance by providing segmented point cloud from [37], which has shown excellent performance on driving-scene semantic segmentation benchmarks [2].

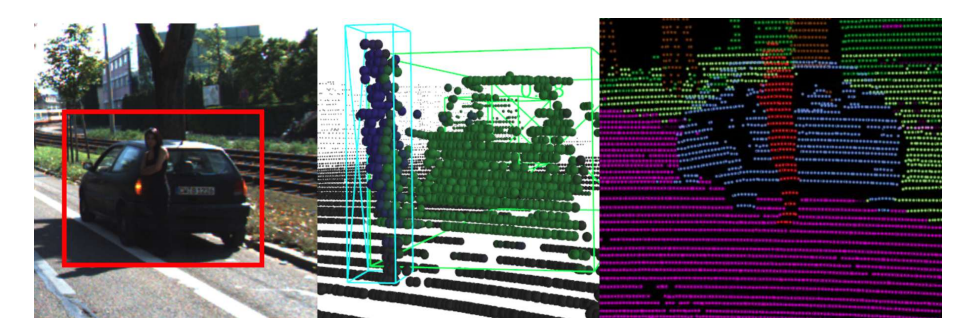


Fig. 1: (left)This depicts a scenario in which two objects, pedestrian and car, are overlapping, causing occlusion. (center)For the pixel-wise segmentation [4] projected onto the point cloud using perspective projection, miss-segmentation occurs in which some of the semantic features of the pedestrian (blue) are classified as car (green). (right)On the other hand, it may be seen that point-wise semantic segmentation has higher accuracy.

2.2 3D Object Detection

Camera-only based 3D object detection. This can be divided into mono, stereo, and multi-view image methods depending on whether they use single or multiple images. In Pseudo-LiDAR [31], depth map from estimated depth creates pseudo-LiDAR. This is utilized as a point cloud, providing geometric information lacking in raw image, and is applied to LiDAR-based detection. D.Park et al. [22] proposed a fully convolutional single-stage 3D detection architecture that combines the pseudo-LiDAR and end-to-end method using mono image as input. It applies FPN (feature pyramid network) [16] as the backbone with three tasks

performed by the head, predicting logit for each class, 2D boxes, and 3D boxes. BEVFormer [15] is based on the transformer and attention mechanism to multiview images. To mitigate the increase in computational cost due to the larger input dimension when using multiple camera views, BEV features from 2D images are utilized. It conducts spatial cross-attention between multi-camera views to connect the same objects across different camera views and extract spatial information as a grid-shaped BEV query. By receiving video inputs instead of static images, it detects moving objects and those heavily occluded, then combines spatial and temporal information extracted through the attention layer for use. However, due to the fundamental characteristics of image, inaccurate estimated depth can interfere with detection performance. In other words, this method can suffer from efficiency issues compared to LiDAR-based detection as concatenating multiple images increases the input dimension, leading to higher computational cost and lower performance.

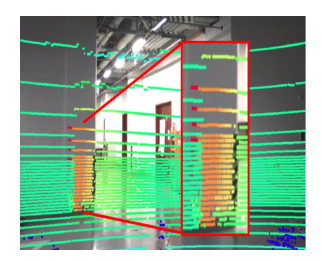




Fig. 2: (left)Due to the error-sensitive hard association based on the LiDAR-camera calibration matrix, some points were not projected onto reflective surfaces. (right)Additionally, many image features did not correspond to the point cloud. it is stated that less than 5% of image features match with point clouds (for a 32-channel LiDAR scanner) [18]

multi-modal 3D object detection. Based on above, multi-modal 3D detection has been proposed, and fusion methods are categorized into early, intermediate, and late fusion based on the stages of fusion. In early fusion, data existing in different coordinates are transformed to be combined. In [30], pixel-wise semantic feature obtained from 2D semantic segmentation is concatenated with raw point cloud and applied to 3D object detection, aiming to supplement semantic feature lacking in point cloud. Intermediate fusion involves fusing features obtained through backbone networks separately for point clouds and images. Z.Liu et al. [18] proposed a method where both features are represented in a unified representation on BEV and performs both 3D detection and BEV map segmentation based on fused features on the representation. AVOD [13] and MV3D [8] aggregate features extracted from images and point cloud to generate 3D proposals, which serve as inputs to the RPN(region proposal network) for 3D object detection. Late fusion involves fusing high-level data obtained from

processing different sensors. CLOCs [21] aims to improve detection performance by fusing 2D bounding boxes obtained from 2D detector and 3D bounding boxes obtained from 3D detector. However, such multimodal 3D object detection poses additional challenge, as it requires considering various representations defined in different domain as a unified representation and demands synchronization for actual implementation. In the process of considering unified representation, it requires the calibration matrix between LiDAR and camera, and even slight errors in this matrix can significantly impact performance. And also in Fig. 2, semantic loss can occur due to an insufficient number of point clouds matching pixels.

LiDAR-only based 3D object. Methods that directly utilize point cloud without voxelization or sampling can preserve spatial features. For example, PointRCNN [27] is a two-stage detector composed of region proposal, classification, and box regression. It uses PointNet++ [25] as the backbone network to obtain point-wise feature vectors from an encoder and decoder. These vectors are utilized for 3D proposal generation and foreground point segmentation, resulting in semantic features and foreground masks, respectively. Merged them with raw point cloud, region pooling returns semantic features and local spatial points. Finally, 3D boxes of detected objects are returned after refinement and confidence prediction. SECOND [34], which utilizes voxel grouping for point cloud on a 3D grid, was proposed to address issues like computational cost increase due to sparsity in VoxelNet [36] and low performance in predicting orientation. Unlike the 3D dense convolutional neural network in [36], the sparse convolutional neural network in [34] considers only non-zero data and optimizes convolution operations through fast rule generation for repetitive patterns. This optimization greatly enhances speed during training and inference. On the other hand, Point-Pillars [14] utilizes representation defined in 2D grid along with the corresponding feature map, enabling it to apply only 2D convolutions for highly efficient operations. However, these methods primarily focus on detecting the presence of objects in the scene, leading to limitation in obtaining context information between points. Therefore, LiDAR-only based 3D detection has inconsistency between localization and classification of 3D bounding boxes [11].

3 Method

3.1 3D Semantic Segmentation with Cylinder3D

Cylindrical coordinate transformation. This method is proposed considering that point clouds obtained in outdoor environments exhibit various densities. Unlike Cartesian coordinate, Cylindrical coordinate allows grid that increase from the reference point to include point clouds that are further away. This enables point clouds to be evenly distributed across different regions, unlike Cartesian coordinate. Additionally, unlike 2D projection, it preserves 3D representation inherent in point clouds. The transformed point cloud is passed

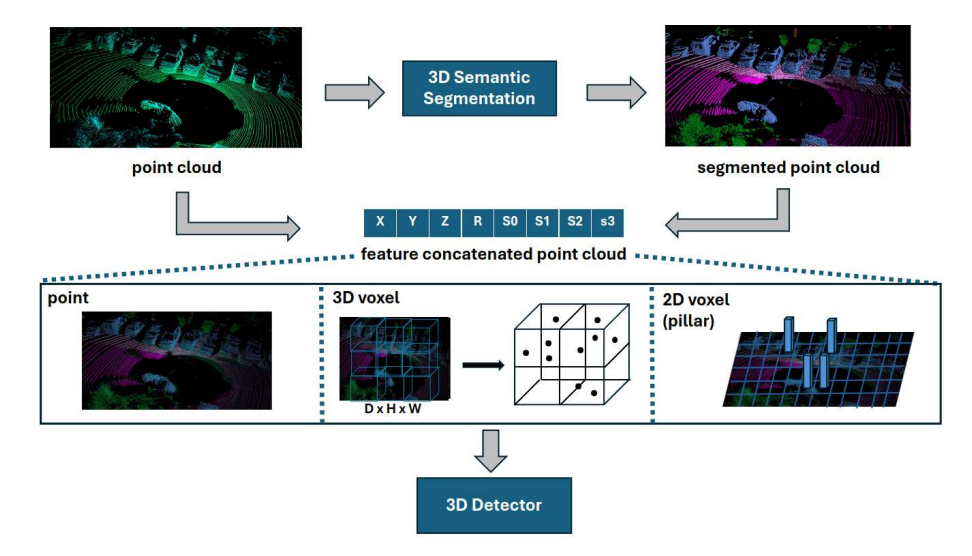


Fig. 3: Overview of SeSame. Point cloud is concatenated with the segmented result and serves as the input to the point encoder of detectors. This can be applied to various feature extractors used by each detector.

through a simplified, MLP-based PointNet [24] to return cylinder features.

Asymmetrical Residual Block. This module, designed to reduce computation costs, serves as a basic component for extracting features through downsampling and fusing low-level features through upsampling. Each block consists of 3D convolution and 3D deconvolution with a stride of 2. The asymmetric residual block returns a receptive field of the same size as the kernel with $3\times3\times3$ in 3D convolution. Asymmetric residuality is achieved by composing 3D convolutions with kernel of $1\times3\times3$ and $3\times1\times3$.

DDCM: Dimension-Decomposition based on Context Modeling. Point clouds exhibit large diversity in context between point clouds acquired from different scenes. To encode these context features, the context must be a high-rank tensor. However, modeling high-rank contexts incurs significant costs [6]. Therefore, the context features of point cloud are decomposed into low-rank forms, and then rank-1 kernels are applied to the three dimensions: height, width, and depth. The sigmoid function regulates the results obtained from the three convolutions to generate weights for each dimension. By aggregating the three low-rank activations, the final context feature obtained becomes a high-rank context feature. The DDCM contributes to efficiency in obtaining it through dimension decomposition.

3.2 Feature Concatenation

Motivation. We were highly motivated by [30]. In the paper, semantic features obtained from stereo images were matched and then concatenated to the point cloud. These features were mapped to three classes at the pixel-wise level, derived from a 2D semantic segmentation [5]. However, this matching was based on perspective projection, which can cause loss and distortion as mentioned earlier. Therefore, we utilize semantic information directly extracted from the point cloud, preserving 3D geometric information without such projection.

Proposed Method.

Algorithm 1 Semantic Feature Concatenation for Point Cloud

```
Input: label map: m(i,class), point cloud: P = \{p_i = (x_i, y_i, z_i, r_i) | i = 1, ..., n\}
Output: segmented point cloud : P_L = \{p_i^L = (x_i, y_i, z_i, r_i, s0_i, s1_i, s2_i, s3_i) | i = \{p_i^L = (x_i, y_i, z_i, r_i, s0_i, s1_i, s2_i, s3_i) | i = \{p_i^L = (x_i, y_i, z_i, r_i, s0_i, s1_i, s2_i, s3_i) | i = \{p_i^L = (x_i, y_i, z_i, r_i, s0_i, s1_i, s2_i, s3_i) | i = \{p_i^L = (x_i, y_i, z_i, r_i, s0_i, s1_i, s2_i, s3_i) | i = \{p_i^L = (x_i, y_i, z_i, r_i, s0_i, s1_i, s2_i, s3_i) | i = \{p_i^L = (x_i, y_i, z_i, r_i, s0_i, s1_i, s2_i, s3_i) | i = \{p_i^L = (x_i, y_i, z_i, r_i, s0_i, s1_i, s2_i, s3_i) | i = \{p_i^L = (x_i, y_i, z_i, r_i, s0_i, s1_i, s2_i, s3_i) | i = \{p_i^L = (x_i, y_i, z_i, r_i, s0_i, s1_i, s2_i, s3_i) | i = \{p_i^L = (x_i, y_i, z_i, r_i, s0_i, s1_i, s2_i, s3_i) | i = \{p_i^L = (x_i, y_i, z_i, s1_i, s2_i, s3_i) | i = \{p_i^L = (x_i, y_i, z_i, s1_i, s2_i, s3_i) | i = \{p_i^L = (x_i, y_i, s1_i, s2_i, s3_i) | i = \{p_i^L = (x_i, y_i, s1_i, s2_i, s3_i) | i = \{p_i^L = (x_i, y_i, s1_i, s2_i, s3_i) | i = \{p_i^L = (x_i, y_i, s1_i, s2_i, s3_i) | i = \{p_i^L = (x_i, y_i, s1_i, s1
      1: procedure ConcatSemFeature(m, P)
      2:
                                         P_L \leftarrow \{\}
                                        for all i, point \in P do
     3:
                                                             label sem \leftarrow \mathbf{Cylinder3D}(point)
      4:
                                                             label \ onehot \leftarrow \mathbf{Sem2KITTI}(m(i, label \ sem))
     5:
      6:
                                                             p_i^{\mathrm{L}} \leftarrow \mathbf{Concat}(point, label\_onehot)
                                                              P_L \leftarrow P_L \cup p_i^{\mathrm{L}}
      7:
                                        end for
     8:
    9:
                                        return P_L
10: end procedure
```

As shown in Algorithm 1, the semantic features from Cylinder3D [37] include an information per each point, indicating which class it belongs to. This corresponds to the semantic label map in the training dataset of [37], SemanticKITTI [2], and class mapping is applied to detectors trained on KITTI 3D object detection dataset. Among the semantic segmentation, only classes corresponding to the KITTI label map are assigned, followed by one-hot encoding. This returns 1×4 tensor, for example, if a point is classified as a car, 1 is assigned to s1, and 0 is assigned to others. After aggregating with the raw point cloud, the following concatenated feature is generated for a point: $[x_i, y_i, z_i, r_i, s0_i, s1_i, s2_i, s3_i]$, where i is index number. Here, $s0 \sim s3$ represent semantic information for unlabeled, car, pedestrian, and cyclist, respectively. The concatenated feature obtained in this way becomes the input of feature extractor of each detectors.

3.3 3D Object Detection varying with Encoding Method

PointRCNN. The feature concatenated point cloud is passed through the backbone network [25], to extract point-wise features. Concurrently, contextual information is obtained through foreground segmentation, and 3D box proposals

are generated. For 3D bounding box regression, the foreground point area is discretized into bins along the x and z axes in the LiDAR coordinate system. The size of each bin along each axis is determined by the coordinates defined within the region of interest of the foreground points and the centroid coordinate of the region. Based on this, similar to [23], the orientation and size of the 3D bounding box are estimated. To better local spatial features for these proposals, they are refined based on the canonical transform and loss function defined on the 3D ground-truth box.

SECOND. Inspired by [36], this propose a method that considers only meaningful voxels in the input point cloud. A limited number of voxels are defined in a buffer, and each individual point within the point cloud is assigned to the associated voxel, which has local coordinates within the voxel. Taking into account the distribution of points, the region where the maximum number of points existing within a voxel is defined according to the object class. The point cloud, encoded into 3D voxels, is passed through FCN [19], batch normalization, and ReLU to return point-wise features. The locally aggregated features for each voxel, obtained through element-wise max pooling, are concatenated with the previously obtained point-wise features. This feature is then transformed into a column matrix through im2col operation. Subsequently, considering the sparsity of the point cloud, a rule matrix is defined based on 3D rule generation to gather necessary inputs. This is done to consider only meaningful inputs. Finally, through optimized operations based on GEMM (General Matrix to Matrix Multiplication)-convolution, the RPN predicts class, regression offset, and direction.

PointPillars. To apply 2D convolution to the point cloud, pillar feature net generate a pseudo image. This discretizes points uniformly on a grid in the x-y plane without limit along the z-axis in 3D space. The generated pillars are encoded with a dimensionality of D = 9, representing $(x, y, z, r, x_c, y_c, z_c, x_p, y_p)$, where the subscript c and p denote the distance to the arithmetic mean of all points in the pillar and the offset from the x, y center of the pillar, respectively. This results in a tensor of size (D, P, N), where P is the number of nonempty pillars per sample, and N is the number of points per individual pillar. If there is either too much or too little data in a pillar, random sampling or zero padding is applied, respectively. After passing through Batch Normalization and ReLU(Rectified Linear Unit), the tensor is transformed into a final tensor of size (C, P, N), where C represents the number of channels. Subsequently, max pooling is applied to convert it into a tensor of size (C, P), which is then reshaped to form a pseudo image of size (C, H, W) where H and W represent the height and width. And the image passes through 2D CNN backbone. The backbone consists of two sub-networks: a top-down network generating features with progressively smaller spatial resolution, and a second network responsible for upsampling and aggregating these top-down features. This forms the input to the Single Shot

Detector(SSD) [17] detection head, from which predicted 2D boxes are matched with ground truth using 2D IoU(intersection-over-union) [9].

3.4 Loss Functions

3D Semantic Segmentation. For network optimization, weighted cross-entropy loss and a lovasz-softmax [3] loss are applied to maximize per point accuracy and IoU score for all classes. They share the same weight. So, the total loss is a summation of them.

3D Object Detection.

- **PointRCNN.** In stage 1, focal loss was applied to address class-imbalance because background points, obtained through foreground segmentation, are more numerous than foreground points. For bin-based classification in 3D box generation, cross-entropy loss was applied for the x and z axes and orientation, while Smooth L1 loss was used for regression based on residual values for the y axis and object dimensions (h, w, l). In stage 2, during the refinement process, a positive label is assigned if the IoU is 0.55 or higher; otherwise, it is considered a negative label. Refinement is applied solely to proposals with positive labels, and cross-entropy loss is computed accordingly.
- **SECOND, PointPillars.** Ground truth and anchor boxes are defined as (x, y, z, w, h, l, theta). Localization loss is calculated through Smooth L1 loss for the residual between these two boxes. The probability associated with each anchor serves as an argument for the focal loss applied in calculating the classification loss. Additionally, directional loss is added to these two losses to compute the final loss.

4 Experiment

Training Details. SeSame+point, +voxel, and +pillar are trained with learning rates of 0.01, 0.003, and 0.003, and batch sizes of 8, 16, and 16, respectively. All three detectors share the same Adam as optimizer and OneCycleLR as scheduler [29], with a weight decay rate of 0.01 and momentum of 0.9, and are trained for 80 epochs with a single TITAN RTX GPU.

SemanticKITTI. Cylinder3D was trained on the SemanticKITTI dataset, which consists of point clouds classified into 28 classes. They are merged into a total of 19 classes by combining classes based on different moving statuses and ignoring classes with too few points. The label data containing this information is of uint32_t, where the upper half represents the instance label and the lower half represents the semantic label. In this paper, only the lower half containing semantic labels from this data was used. The 19 classes were mapped to three

classes defined in the KITTI object detection benchmark dataset: car, pedestrian, and cyclist.

KITTI 3D Object Detection Evaluation. The dataset contains 7481 training samples and 7518 testing samples, consisting of images and LiDAR point clouds. All existing detectors [14,27,34] use the dataset, but differ in data split. In this paper, following general split method, the given training dataset was further split into 3712 training and 3769 validation samples for experiment. The train and val samples obtained through this split do not overlap [7]. Before the splitting, pretrained Cylinder3D is used to perform inference on this dataset, and the resulting label mapped to the KITTI dataset is concatenated with training sample, thus forming the training dataset. The same approach was applied to the test split, and the results were submitted to the official test server, showing the outcomes as in Tabs. 1 and 2. The evaluation metric used was Average Precision (AP), with IoU thresholds of 0.7 for cars and 0.5 for pedestrians and cyclists, respectively. The three classes are divided into easy, moderate, and hard based on detection difficulty, where occlusion and truncation increase from the former to the latter.

Data Augmentation. Due to the limited number of training samples in the dataset, common data augmentation techniques applied in existing detectors are incorporated. Following the approach initiated from [36], a database is first created from the given training dataset and its labels. Random selection is made from this database for training, involving data augmentation such as random flipping along the x-axis, rotation around the z-axis and the origin within the range of $[-\pi/4, \pi/4]$, and random scaling within the range of [0.95, 1.05]. These augmentations are applied to both the parameters of individual bounding boxes and the point sets within those boxes, being configured differently for each detector. To fairly evaluate the effectiveness of the proposed method, common settings are referenced and applied uniformly. If the 3D bounding boxes and point clouds generated by this technique result in physically implausible scenarios, such as collision due to overlapping bounding boxes, the original data is reverted.

4.1 Overall Results

The results are based on the evaluation detection metrics which are: BEV, 3D as shown in Tabs. 1 and 2. The proposed method is applied to three detectors classified based on the type of input features, outperforming both the camera-only method and the multi-modality method. Among these detectors, when using point feature as input, it outperforms the baseline detector on car. This result is evident in both metrics, which signifies the consistency of the results. As mentioned in [14], increasing per box data augmentation leads to a further degradation in performance for pedestrians. This was also observed in our result. A comparison with before and after the application of the proposed method, can be seen in Sec. 4.2.



Fig. 4: The leftmost of the four sections represents the ground truth(GT), while the remaining three sections depict predictions from detectors based on input features of point [27], voxel [34], and pillar [14]. The top figure illustrates a scenario with multiple cars(blue) and some cyclists(red), while the bottom figure shows multiple pedestrians(green).

Table 1: Results on the KITTI test 3D detection benchmark

Method	modality	Car (IoU=0.7)			Pedestrian (IoU=0.5)			Cyclist (IoU=0.5)		
Method		easy	mod	hard	easy	mod	hard	easy	mod	hard
DD3D [22]	Camera (Mono)	23.22	16.34	14.20	13.91	9.30	8.05	2.39	1.52	1.31
Pseudo-LiDAR $[31]$ + AVOD $[13]$	Camera (Stereo)	55.4	37.2	31.4	N/A	N/A	N/A	N/A	N/A	N/A
MV3D [8]	LiDAR + Camera	71.09	62.35	55.12	N/A	N/A	N/A	N/A	N/A	N/A
AVOD-FPN [13]	LiDAR + Camera	73.59	65.78	58.38	38.28	31.51	26.98	60.11	44.90	38.80
PointRCNN [27]	LiDAR (point)	85.94	75.76	68.32	49.43	41.78	38.63	73.93	59.60	53.59
SECOND [34]	LiDAR (voxel)	83.13	73.66	66.20	51.07	42.56	37.29	70.51	53.85	46.90
PointPillars [14]	LiDAR (pillar)	79.05	74.99	68.30	52.08	43.53	41.49	75.78	59.07	52.92
SeSame + point (Ours)	LiDAR (point)	85.25	76.83	71.60	42.29	35.34	33.02	69.55	54.56	48.34
SeSame + voxel (Ours)	LiDAR (voxel)	81.51	75.05	70.53	46.53	37.37	33.56	70.97	54.36	48.66
SeSame + pillar (Ours)	LiDAR (pillar)	83.88	73.85	68.65	37.61	31.00	28.86	64.55	51.74	46.13

Table 2: Results on the KITTI test BEV detection benchmark

Method	modality	Car (IoU=0.7)			Pedestrian (IoU=0.5)			Cyclist (IoU=0.5)		
		easy	mod	hard	easy	mod	hard	easy	mod	hard
DD3D [22]	Camera (Mono)	30.98	22.56	20.03	15.90	10.85	8.05	3.20	1.99	1.79
Pseudo-LiDAR $[31]$ + AVOD $[13]$	Camera (Stereo)	66.8	47.2	40.3	N/A	N/A	N/A	N/A	N/A	N/A
MV3D [8]	LiDAR + Camera	86.02	76.90	68.49	N/A	N/A	N/A	N/A	N/A	N/A
AVOD-FPN [13]	${\rm LiDAR} + {\rm Camera}$	88.53	83.79	77.90	58.75	51.05	47.54	68.06	57.48	50.77
PointRCNN [27]	LiDAR (point)	92.13	87.39	82.72	54.77	46.13	42.84	82.56	67.24	60.28
SECOND [34]	LiDAR (voxel)	89.39	83.77	78.59	55.99	45.02	40.93	76.5	56.05	49.45
PointPillars [14]	LiDAR (pillar)	90.07	86.56	82.81	<u>57.60</u>	48.64	45.78	79.90	62.73	55.58
SeSame + point (Ours)	LiDAR (point)	90.84	87.49	83.77	48.25	41.22	39.18	75.73	61.70	55.27
SeSame + voxel (Ours)	LiDAR (voxel)	89.86	85.62	80.95	50.12	41.59	37.79	76.95	59.36	53.14
${f SeSame + pillar (Ours)}$	LiDAR (pillar)	90.61	86.88	81.93	44.21	37.31	35.17	72.22	60.21	53.67

4.2 Ablation Study

Encoding: Label and Score. The label obtained from 3D semantic segmentation is mapped from SemanticKITTI to KITTI, resulting in a feature vector composed of 0 or 1 according to one-hot encoding. When comparing the feature

concatenated point cloud with the point cloud passed through softmax for score mapping, the accuracy improved slightly by +0.1 for the score mapping with val split. However, for test split, the accuracy was higher when mapped by one-hot encoding label. Furthermore, there was a discrepancy in performance obtained from the val split and the test split when mapped by score. This implies that the training was within the range of noise for score mapping, and mapping by label is more reasonable.

Comparison Before and After Application of Proposed Method.

When comparing the method applied detectors with their base, the results are as follows: they all show performance improvements for cars, especially with SECOND using voxel features as input showing the most benefit as in Tab. 3. This improvement is also observed for cyclists, with a slight gain in 3D detection and a larger gain in BEV. When voxel features used as input, performance gains are observed not only for cars but also for cyclists. [14] did not show gains in identifying pedestrians and cyclists. Unlike this, [34] also includes a similar sampling process, but it showed performance gains for cyclists. For [34], the 3D point cloud is converted into a 3D voxel grid, and then VFE(voxel feature extractor) extracts semantic features. However, for [14], the point cloud is projected onto BEV plane and 2D backbone extracts the features. The backbone may have limitation in extracting semantic features compared to VFE. Additionally, the feature concatenated point cloud projected in 2D makes it difficult to utilize semantic features. Therefore, there is a limitation in achieving a better mAP even with sufficient mean of Intersection over Union (mIoU) provided by the semantic segmentation.

Table 3: Performance comparison before and after applying the proposed method based on the KITTI object detection benchmark with IoU threshold 0.7. Detectors to which the method was applied all showed performance improvement.

Method	modality		AP_{3D}		AP_{BEV}			
Method	modanty	easy	mod	hard	easy	mod	hard	
PointRCNN [27]	LiDAR (point)	86.96	75.64	70.70	92.13	87.39	82.72	
SeSame+Point (Ours)	LiDAR (point)	85.25	76.83	71.60	90.84	87.49	83.77	
$\it \Delta$		-1.71	1.19	0.9	-1.29	0.1	1.05	
SECOND [34]	LiDAR (voxel)	83.13	73.66	66.20	88.07	79.37	77.95	
SeSame+Voxel (Ours)	LiDAR (voxel)	81.51	75.05	70.53	89.86	85.62	80.95	
Δ		-1.62	1.39	4.33	1.79	6.25	3.00	
PointPillars [14]	LiDAR (pillar)	79.05	74.99	68.30	88.35	86.10	79.83	
SeSame+Pillar (Ours)	LiDAR (pillar)	83.88	73.85	68.65	90.61	86.88	81.93	
Δ		4.83	-1.14	0.35	2.26	0.78	2.10	

Comparison between Reference Method and Ours.

14 H.O, K.Huh

We are inspired by PointPainting [30], which is based on multimodal. There is only result of painted PointRCNN on test split, we compared it with SeSame+point as in Tab. 4. In terms of car, PointPainting showed a slight improvement in performance on BEV and our method exhibited superior performance improvement on 3D detection. However, PointPainting performed better for pedestrians and cyclists. We speculate that this is because point clouds inherently have sparsity, which is more pronounced for specific objects (pedestrians, cyclists). In other words, for objects that are small in size and have enhanced sparsity, image-based semantic features are more effective to guarantee density. Thus, the LiDAR semantic segmentation can provide reliable semantic features for car, but may not for pedestrian and cyclist. For this reason, future research focuses on a multimodal 3D semantic segmentation that considers both point cloud and image, taking into account various objects on the road.

Table 4: Performance comparison of BEV and 3D object detection with reference method and ours for the car class on test split. The IoU threshold is 0.7.

Method	Modality	$\mathrm{AP_{3D}}$			AP_{BEV}			
Method	Modanty	Easy	Mod	od Hard Easy Mo	Mod	Hard		
painted PointRCNN [30]	LiDAR (point)	82.11	71.70	67.08	92.45	88.11	83.36	
SeSame+Point (Ours)	LiDAR (point)	$\bf 85.25$	76.83	71.60	90.84	87.49	83.77	

5 Conclusion

Single-modality 3D object detection is necessary as a fallback for sensor fault that occur during the execution of the multi-modality task on autonomous driving. To overcome the lack of semantic information, we utilize semantic features obtained from 3D semantic segmentation for LiDAR-only 3D object detection. These are concatenated to point clouds and applied to three detectors classified according to the input feature: point, voxel, and pillar. We demonstrate the potential for 3D semantic segmentation to be utilized in 3D object detection, resulting in performance gains for cars. However, there is limitation for pedestrians and cyclists due to the inherent sparsity of point cloud. LiDAR-based 3D semantic segmentation can ensure performance improvement in 3D object detection for objects with minimal sparsity, while for other objects, there is a need to utilize camera modality that guarantees density. In conclusion, future research on multimodal 3D semantic segmentation will consider both geometric and semantic information inherent in point clouds and images each other. Furthermore, we aim to apply this to 3D object detection to achieve even better performance improvements.

References

- Bai, X., Hu, Z., Zhu, X., Huang, Q., Chen, Y., Fu, H., Tai, C.L.: Transfusion: Robust lidar-camera fusion for 3d object detection with transformers. In: Proceedings of the IEEE/CVF Conference on Computer Vision and Pattern Recognition (CVPR). pp. 1090–1099 (June 2022) 3
- Behley, J., Garbade, M., Milioto, A., Quenzel, J., Behnke, S., Stachniss, C., Gall, J.: Semantickitti: A dataset for semantic scene understanding of lidar sequences. In: Proceedings of the IEEE/CVF International Conference on Computer Vision (ICCV) (October 2019) 4, 8
- 3. Berman, M., Triki, A.R., Blaschko, M.B.: The lovász-softmax loss: A tractable surrogate for the optimization of the intersection-over-union measure in neural networks. In: Proceedings of the IEEE Conference on Computer Vision and Pattern Recognition (CVPR) (June 2018) 10
- Chen, L., Papandreou, G., Schroff, F., Adam, H.: Rethinking atrous convolution for semantic image segmentation. CoRR abs/1706.05587 (2017), http://arxiv. org/abs/1706.05587 4
- Chen, L.C., Zhu, Y., Papandreou, G., Schroff, F., Adam, H.: Encoder-decoder with atrous separable convolution for semantic image segmentation. In: Proceedings of the European Conference on Computer Vision (ECCV) (September 2018) 8
- Chen, W., Zhu, X., Sun, R., He, J., Li, R., Shen, X., Yu, B.: Tensor Low-Rank Reconstruction for Semantic Segmentation. In: Vedaldi, A., Bischof, H., Brox, T., Frahm, J.M. (eds.) Computer Vision – ECCV 2020. pp. 52–69. Springer International Publishing, Cham (2020) 7
- Chen, X., Kundu, K., Zhu, Y., Berneshawi, A.G., Ma, H., Fidler, S., Urtasun, R.: 3D Object Proposals for Accurate Object Class Detection. In: Cortes, C., Lawrence, N., Lee, D., Sugiyama, M., Garnett, R. (eds.) Advances in Neural Information Processing Systems. vol. 28. Curran Associates, Inc. (2015), https://proceedings.neurips.cc/paper_files/paper/2015/file/6da37dd3139aa4d9aa55b8d237ec5d4a-Paper.pdf 11
- 8. Chen, X., Ma, H., Wan, J., Li, B., Xia, T.: Multi-view 3d object detection network for autonomous driving. In: Proceedings of the IEEE Conference on Computer Vision and Pattern Recognition (CVPR) (July 2017) 2, 5, 12
- Everingham, M., Gool, L.V., Williams, C.K.I., Winn, J.M., Zisserman, A.: The pascal visual object classes (voc) challenge. Int. J. Comput. Vis. 88(2), 303–338 (2010), http://dblp.uni-trier.de/db/journals/ijcv/ijcv88.html#EveringhamGWWZ10 10
- 10. Hao, S., Zhou, Y., Guo, Y.: A Brief Survey on Semantic Segmentation with Deep Learning. Neurocomputing 406, 302-321 (2020). https://doi.org/https://doi.org/10.1016/j.neucom.2019.11.118, https://www.sciencedirect.com/science/article/pii/S0925231220305476 3
- Huang, T., Liu, Z., Chen, X., Bai, X.: EPNet: Enhancing Point Features with Image Semantics for 3D Object Detection. In: Vedaldi, A., Bischof, H., Brox, T., Frahm, J.M. (eds.) Computer Vision – ECCV 2020. pp. 35–52. Springer International Publishing, Cham (2020) 2, 6
- 12. Iandola, F.N., Han, S., Moskewicz, M.W., Ashraf, K., Dally, W.J., Keutzer, K.: Squeezenet: Alexnet-level accuracy with 50x fewer parameters and <0.5mb model size (2016) 3
- 13. Ku, J., Mozifian, M., Lee, J., Harakeh, A., Waslander, S.L.: Joint 3d proposal generation and object detection from view aggregation. In: 2018 IEEE/RSJ Inter-

- national Conference on Intelligent Robots and Systems (IROS). pp. 1–8 (2018). https://doi.org/10.1109/IROS.2018.8594049 2, 5, 12
- Lang, A.H., Vora, S., Caesar, H., Zhou, L., Yang, J., Beijbom, O.: PointPillars: Fast encoders for object detection from point clouds. Proceedings of the IEEE Computer Society Conference on Computer Vision and Pattern Recognition 2019-June, 12689–12697 (2019). https://doi.org/10.1109/CVPR.2019.01298 6, 11, 12, 13
- Li, Z., Wang, W., Li, H., Xie, E., Sima, C., Lu, T., Qiao, Y., Dai, J.: BEV-Former: Learning Bird's-Eye-View Representation from Multi-camera Images via Spatiotemporal Transformers. In: Avidan, S., Brostow, G., Cissé, M., Farinella, G.M., Hassner, T. (eds.) Computer Vision ECCV 2022. pp. 1–18. Springer Nature Switzerland, Cham (2022) 5
- Lin, T.Y., Dollar, P., Girshick, R., He, K., Hariharan, B., Belongie, S.: Feature pyramid networks for object detection. In: Proceedings of the IEEE Conference on Computer Vision and Pattern Recognition (CVPR) (July 2017) 4
- Liu, W., Anguelov, D., Erhan, D., Szegedy, C., Reed, S., Fu, C.Y., Berg, A.C.: SSD: Single Shot MultiBox Detector. In: Leibe, B., Matas, J., Sebe, N., Welling, M. (eds.) Computer Vision – ECCV 2016. pp. 21–37. Springer International Publishing, Cham (2016) 10
- Liu, Z., Tang, H., Amini, A., Yang, X., Mao, H., Rus, D.L., Han, S.: Bevfusion: Multi-task multi-sensor fusion with unified bird's-eye view representation. In: 2023 IEEE International Conference on Robotics and Automation (ICRA). pp. 2774–2781 (2023). https://doi.org/10.1109/ICRA48891.2023.10160968 2, 5
- 19. Long, J., Shelhamer, E., Darrell, T.: Fully convolutional networks for semantic segmentation. In: Proceedings of the IEEE Conference on Computer Vision and Pattern Recognition (CVPR) (June 2015) 3, 9
- 20. Ma, Y., Wang, T., Bai, X., Yang, H., Hou, Y., Wang, Y., Qiao, Y., Yang, R., Manocha, D., Zhu, X.: Vision-Centric BEV Perception: A Survey (aug 2022), http://arxiv.org/abs/2208.02797 2
- Pang, S., Morris, D., Radha, H.: CLOCs: Camera-LiDAR Object Candidates Fusion for 3D Object Detection. In: IEEE International Conference on Intelligent Robots and Systems. pp. 10386–10393 (2020). https://doi.org/10.1109/IROS45743.2020.9341791 2, 6
- 22. Park, D., Ambruş, R., Guizilini, V., Li, J., Gaidon, A.: DD3D: Is Pseudo-Lidar needed for Monocular 3D Object detection? Proceedings of the IEEE International Conference on Computer Vision pp. 3122–3132 (2021). https://doi.org/10.1109/ICCV48922.2021.00313 4, 12
- 23. Qi, C.R., Liu, W., Wu, C., Su, H., Guibas, L.J.: Frustum pointnets for 3d object detection from rgb-d data. In: Proceedings of the IEEE Conference on Computer Vision and Pattern Recognition (CVPR) (June 2018) 2, 9
- 24. Qi, C.R., Su, H., Mo, K., Guibas, L.J.: Pointnet: Deep learning on point sets for 3d classification and segmentation. In: Proceedings of the IEEE Conference on Computer Vision and Pattern Recognition (CVPR) (July 2017) 3, 7
- 25. Qi, C.R., Yi, L., Su, H., Guibas, L.J.: PointNet++: Deep hierarchical feature learning on point sets in a metric space. In: Advances in Neural Information Processing Systems. vol. 2017-Decem, pp. 5100–5109 (2017) 3, 6, 8
- Ronneberger, O., Fischer, P., Brox, T.: U-Net: Convolutional Networks for Biomedical Image Segmentation. In: Navab, N., Hornegger, J., Wells, W.M., Frangi, A.F. (eds.) Medical Image Computing and Computer-Assisted Intervention MICCAI 2015. pp. 234–241. Springer International Publishing, Cham (2015) 3

- 27. Shi, S., Wang, X., Li, H.: PointRCNN: 3D object proposal generation and detection from point cloud. In: Proceedings of the IEEE Computer Society Conference on Computer Vision and Pattern Recognition. vol. 2019-June, pp. 770–779 (2019). https://doi.org/10.1109/CVPR.2019.00086 6, 11, 12, 13
- 28. Singh, A., Bankiti, V.: Surround-View Vision-based 3D Detection for Autonomous Driving: A Survey (2023), http://arxiv.org/abs/2302.06650 2
- 29. Smith, L.N.: A disciplined approach to neural network hyper-parameters: Part 1 learning rate, batch size, momentum, and weight decay (2018) 10
- 30. Vora, S., Lang, A.H., Helou, B., Beijbom, O.: PointPainting: Sequential fusion for 3D object detection. Proceedings of the IEEE Computer Society Conference on Computer Vision and Pattern Recognition pp. 4603–4611 (2020). https://doi.org/10.1109/CVPR42600.2020.00466 2, 5, 8, 14
- 31. Wang, Y., Chao, W.L., Garg, D., Hariharan, B., Campbell, M., Weinberger, K.Q.: Pseudo-lidar from visual depth estimation: Bridging the gap in 3D object detection for autonomous driving. Proceedings of the IEEE Computer Society Conference on Computer Vision and Pattern Recognition 2019-June, 8437–8445 (2019). https://doi.org/10.1109/CVPR.2019.00864 2, 4, 12
- 32. Wang, Y., Shi, T., Yun, P., Tai, L., Liu, M.: Pointseg: Real-time semantic segmentation based on 3d lidar point cloud (2018) 3
- Wu, B., Wan, A., Yue, X., Keutzer, K.: Squeezeseg: Convolutional neural nets with recurrent crf for real-time road-object segmentation from 3d lidar point cloud. In: 2018 IEEE International Conference on Robotics and Automation (ICRA). pp. 1887–1893 (2018). https://doi.org/10.1109/ICRA.2018.8462926
- 34. Yan, Y., Mao, Y., Li, B.: SECOND: Sparsely embedded convolutional detection. Sensors (Switzerland) **18**(10), 1–17 (2018). https://doi.org/10.3390/s181033376, 11, 12, 13
- Zhang, Y., Zhou, Z., David, P., Yue, X., Xi, Z., Gong, B., Foroosh, H.: Polarnet: An improved grid representation for online lidar point clouds semantic segmentation.
 In: Proceedings of the IEEE/CVF Conference on Computer Vision and Pattern Recognition (CVPR) (June 2020) 3
- 36. Zhou, Y., Tuzel, O.: Voxelnet: End-to-end learning for point cloud based 3d object detection. In: Proceedings of the IEEE Conference on Computer Vision and Pattern Recognition (CVPR) (June 2018) 3, 6, 9, 11
- 37. Zhu, X., Zhou, H., Wang, T., Hong, F., Ma, Y., Li, W., Li, H., Lin, D.: Cylindrical and asymmetrical 3d convolution networks for lidar segmentation. In: Proceedings of the IEEE/CVF Conference on Computer Vision and Pattern Recognition (CVPR). pp. 9939–9948 (June 2021) 4, 8
- 38. Zhuang, Z., Li, R., Jia, K., Wang, Q., Li, Y., Tan, M.: Perception-aware multi-sensor fusion for 3d lidar semantic segmentation. In: Proceedings of the IEEE/CVF International Conference on Computer Vision (ICCV). pp. 16280–16290 (October 2021) 3